Kinetic processes of electron beam generated XeF* and Xe_2F* excimers

R. Sauerbrey and W. Walter

Physikalisches Institut der Universität Würzburg, D 8700 Würzburg, West Germany

F. K. Tittel and W. L. Wilson, Jr.

Electrical Engineering Department, Rice University, Houston, Texas 77251
(Received 26 July 1982; accepted 11 October 1982)

Kinetic processes of XeF and Xe_2F have been investigated experimentally in electron beam excited Ar/Xe/NF_3 mixtures. In Xe/NF_3 mixtures no vibrational relaxation was observed in the XeF(B, C) states due to the rapid two-body quenching of XeF(C) by Xe. Two- and three-body quenching constants of XeF(B, C) were measured for several collision partners. An investigation of the Xe_2F production process showed that XeF(C) is the precursor of Xe_2F. Formation and quenching rate constants for Xe_2F have been determined. The kinetic processes of the XeF–Xe_2F system can be described by a relatively simple kinetic model.

I. INTRODUCTION

Kinetic reactions in rare gas halide excimer media have been extensively studied in the last several years. Besides intrinsic scientific interest, these studies have been stimulated by the development of diatomic and triatomic rare gas halide excimer lasers.[1] A detailed understanding of the kinetic processes in such laser media is required for scaling and optimization. The XeF system has recently attracted special interest. Besides the high efficiency XeF laser operating on the $B-X$ transition mainly at 351 and 353 nm,[2–5] laser action has also been achieved on the $C-A$ transition of XeF around 480 nm.[6–12]

Several kinetic studies of the XeF system have been reported for electron beam excited rare gas halide donor mixtures.[13,14] The XeF(B) state can also be very efficiently generated by the photodissociation of XeF_2 with UV radiation. Subsequently, the XeF(C) state is populated by collisions. Therefore, recent work has concentrated on laser experiments[6,11] and kinetic studies[15–20] using photolytic excitation of XeF_2. The XeF system was also studied by direct laser excitation of XeF ground state molecules.[21]

As a result of these numerous investigations, reliable radiative lifetimes for the XeF(B) and the XeF(C) states are now available that agree well with those obtained from theoretical calculations.[22] These experiments revealed the uniqueness of the XeF system as compared to other rare gas halide molecules. Comparatively high two-body quenching constants of XeF(B, C) by rare gases have been measured by several groups that differ in some cases by more than an order of magnitude. This problem was at least partly resolved by the discovery that the XeF(C) state lies about 700 cm^{-1} below the XeF(B) state.[23] The large energy gap between these two states gives rise to collisional coupling effects that depend on such parameters as the nature of buffer gases, buffer gas pressures, or the amount of vibrational relaxation in each electronic state.[18(b)] The collisional coupling between the XeF(B) and the XeF(C) states was only recently taken into account in XeF kinetic studies.[13(b),17–19] Of particular importance are recent experiments reported by Black *et al.*[18] and those by Brashears and Setser[17(b)] because both groups measured two-body quenching constants as well as collisional mixing rate constants for the XeF(B) and the XeF(C) states. Although both investigations contribute considerably to the understanding of the XeF system, there still remains quantitative disagreement of some of the two-body quenching rates, especially the two-body quenching of XeF(C) by xenon.

Furthermore the problem of three-body quenching of XeF(B, C) is still unresolved. The values for three-body quenching constants of XeF by 2Xe, for instance, range from 2.4×10^{-29} cm^6 s^{-1} [15(a)] to no measurable three-body quenching.[17(b)] Therefore, for this process, as well as for some other three-body processes, it is not yet clear if they occur at all and, if they occur, how large their rate coefficients are. The problem of three-body quenching has been complicated by the fact that Xe_2F, the most likely product of a three-body quenching process involving at least one xenon atom, was not observed experimentally despite several attempts.[14,17,18,24] Similar triatomic species are well established for most other rare gas halides.[24–28] The only information available for the XeF–Xe_2F system were theoretical calculations of the potential surfaces of Xe_2F by Huestis.[29] Recently, however, the existence of Xe_2F has been demonstrated by Walter *et al.*[30] and it appears that three-body quenching of XeF by xenon as well as by argon and xenon leads to the formation of Xe_2F.

This work is concerned with an analysis of the quenching processes of XeF with special emphasis on three-body quenching and the formation mechanism of Xe_2F. Experiments have been undertaken using short pulse electron beam excitation of xenon containing rare gas–NF_3 mixtures. Observations of the temporal behavior of the XeF(B, C) and Xe_2F intensities, as well as measurements of the fluorescence yield ratios for the different species, allowed the extraction of the various rate constants. The theoretical framework for this will be outlined in the next section.

 0021-9606/83/020735-13$2.10

II. RATE EQUATIONS AND POTENTIAL SURFACES FOR THE XeF-Xe_2F SYSTEM

For high gas pressures, the vibrational relaxation within the XeF(B) and XeF(C) states is sufficiently fast that the XeF(B, C) system may be described as two states that are mixed by collisions with other species.[18(b)] It is furthermore assumed that Xe_2F is produced from XeF(B, C) by three-body collisions. A kinetic scheme depicting the main reactions for the gas mixture used in the present experiments is shown in Fig. 1. The rate equations for the XeF–Xe_2F systems can then be written as follows:

$$\frac{d[B]}{dt} = P_B + v\cdot[C] - u\cdot[B] - \frac{[B]}{\tau_1} \ , \tag{1}$$

$$\frac{d[C]}{dt} = P_C + u\cdot[B] - v\cdot[C] - \frac{[C]}{\tau_2} \ , \tag{2}$$

$$\frac{d[X]}{dt} = r\cdot[B] + s\cdot[C] - \frac{[X]}{\tau_{eff}} \ , \tag{3}$$

with the following definitions:

$$u = \sum_{i=1}^{n} k_{BC}^{M_i}[M_i] \ , \quad v = \sum_{i=1}^{n} k_{CB}^{M_i}[M_i] \ , \quad \frac{1}{\tau_1} = \frac{1}{\tau_B} + \sum_{i=1}^{n} k_B^{M_i}[M_i] + \frac{1}{2}\sum_{i,j=1}^{n} k_B^{M_iM_j}[M_i][M_j] \ ,$$

$$\frac{1}{\tau_2} = \frac{1}{\tau_C} + \sum_{i=1}^{n} k_C^{M_i}[M_i] + \frac{1}{2}\sum_{i,j=1}^{n} k_C^{M_iM_j}[M_i][M_j] \ , \quad r = \frac{1}{2}\sum_{i,j=1}^{n} k_{BP}^{M_iM_j}[M_i][M_j] \ , \quad s = \frac{1}{2}\sum_{i,j=1}^{n} k_{CP}^{M_iM_j}[M_i][M_j] \ ,$$

$$\frac{1}{\tau_{eff}} = \frac{1}{\tau_X} + \sum_{i=1}^{n} k_X^{M_i}[M_i] \ .$$

Here, $[B]$, $[C]$, and $[X]$ denote the concentrations of XeF(B), XeF(C), and Xe_2F, respectively. P_B and P_C are the production rates for the XeF(B) and the XeF(C) states. The quantities u and v describe the collisional mixing between the B and the C state. $[M_i]$ stands for any collision partner in the gas mixture, mainly Ar, Xe, NF_3, and electrons in the present investigation, and $k_{BC}^{M_i}$ and $k_{CB}^{M_i}$ are the mixing constants for the reaction

$$\mathrm{XeF}(B) + M_i \underset{k_{CB}^{M_i}}{\overset{k_{BC}^{M_i}}{\rightleftharpoons}} \mathrm{XeF}(C) + M_i \ . \tag{4}$$

The B state as well as the C state decay by their respective effective decay frequencies τ_1^{-1} and τ_2^{-1}. These are determined by the probability for radiative decay τ_B^{-1} and τ_C^{-1}, as well as two- and three-body quenching processes. $k_B^{M_i}$, $k_C^{M_i}$ and $k_B^{M_iM_j}$, $k_C^{M_iM_j}$ represent the corresponding two- and three-body quenching constants.

$Xe_2F(3)$ is produced via three-body collisions from XeF(B) and XeF(C) which is described by the quantities r and s. It should be emphasized that the three-body production rate constants $k_{BP}^{M_iM_j}$ and $k_{CP}^{M_iM_j}$ may be different from the corresponding three-body quenching constants $k_B^{M_iM_j}$ and $k_C^{M_iM_j}$. Xe_2F decays by an effective decay frequency τ_{eff}^{-1}, which is given by the sum of the radiative decay probability τ_X^{-1} and a term containing the two-body quenching characterized by two-body quenching constants $k_X^{M_i}$. Three-body quenching of Xe_2F can be neglected as will be shown later.

These rate equations (1)–(3) are, in fact, applicable to any rare gas halide dimer–trimer system up to moderate pumping densities. For considerably smaller energy splitting between the B and the C states which is the case for all other rare gas halide dimers observed up to now, the B and the C states act essentially as one state and Eqs. (1) and (2) can be reduced to one equation. The exact time dependence of P_B and P_C is generally not known. For short pulse e-beam excitation as well as for excitation by short synchrotron radiation pulses,[18] P_B can, however, be approximately treated as a δ function. A direct production of the C state is not observed in photolytic[17,18] or electron beam excitation.[30] Therefore, P_C is neglected compared to C state production via collisions from the B state. The initial conditions for Eqs. (1) and (2) are $B(t=0) = B_0$ and $C(t=0) = 0$ and a solution of Eqs. (1) and (2) can be obtained with[18]

$$B(t) = b_1 e^{\lambda_1 t} + b_2 e^{\lambda_2 t} \ , \tag{5}$$

$$C(t) = c_1(e^{\lambda_1 t} - e^{\lambda_2 t}) \ , \tag{6}$$

where

$$\lambda_{1,2} = -\tfrac{1}{2}(\beta+\gamma) \pm \tfrac{1}{2}[(\beta-\gamma)^2 + 4uv]^{1/2} \ , \quad \beta = u + \frac{1}{\tau_1} \ ;$$

$$\gamma = v + \frac{1}{\tau_2} \ , \tag{7}$$

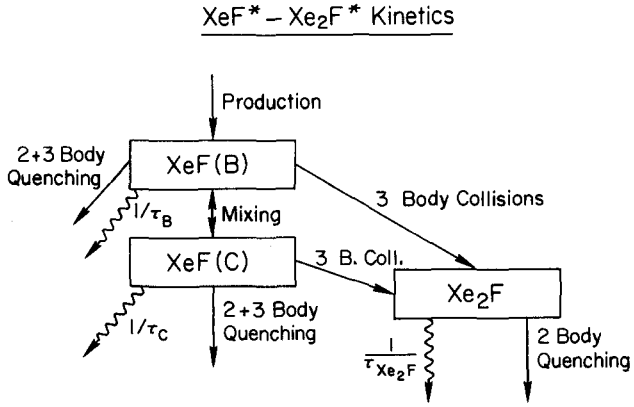

FIG. 1. Important kinetic pathways in the XeF–Xe_2F system for electron beam excitation.

$$K = \tfrac{1}{2}(\beta - \gamma) + \tfrac{1}{2}[(\beta - \gamma)^2 + 4uv]^{1/2} ,$$

$$b_1 \approx \frac{\frac{uv}{K^2}}{1 + \frac{uv}{K^2}} B_0 ; \quad b_2 = \frac{B_0}{1 + \frac{uv}{K^2}} , \quad c_1 = \frac{B_0}{1 + \frac{uv}{K^2}} \frac{u}{K} . \tag{8}$$

The B state first decays with the faster decay frequency $-\lambda_2$ and after equilibrium is reached by collisional mixing both states decay with the slower decay frequency $-\lambda_1$.

For high buffer gas pressure conditions, the mixing processes described by u and v can be considerably faster than all the other decay processes given by τ_1^{-1} and τ_2^{-1}. Under this condition, equilibrium between both states is achieved almost immediately and the expression for the slower decay frequency can be simplified

$$\lambda_1 \approx -\left[\frac{v}{u+v}\frac{1}{\tau_1} + \frac{u}{u+v}\frac{1}{\tau_2}\right] , \quad \text{if } u+v \gg \frac{1}{\tau_1} + \frac{1}{\tau_2} . \tag{9}$$

If one species M_i in the gas mixture strongly dominates the mixing process, one obtains

$$\lambda_1 \approx -\left[\frac{k_{BC}^{M_i}}{k_{BC}^{M_i} + k_{CB}^{M_i}} \cdot \frac{1}{\tau_1} + \frac{k_{BC}^{M_i}}{k_{BC}^{M_i} + k_{CB}^{M_i}} \cdot \frac{1}{\tau_2}\right] . \tag{10}$$

With the solution of Eqs. (1) and (2), Eq. (3) can be solved with the initial condition $X(0) = 0$, yielding a fairly complicated expression. As long as the effective decay times of the dimer states $-\lambda_{1,2}^{-1}$ are shorter than the effective decay time of the trimer τ_{eff}, the temporal shape of the trimer emission is given by a rise time of the order of the width of the dimer pulses and a subsequent exponential decay with the effective lifetime of the trimer. The temporal shape of the trimer emission was analyzed using a computer.

The rate equations (1)–(3) can be converted into equations for the time-integrated intensities of the different species. The time-integrated intensities (fluorescence yield) are given by

$$I_B = \frac{1}{\tau_B}\int_0^\infty B(t)\,dt , \quad I_C = \frac{1}{\tau_C}\int_0^\infty C(t)\,dt ,$$
$$I_X = \frac{1}{\tau_X}\int_0^\infty X(t)\,dt . \tag{11}$$

Setting $P_C = 0$ and considering that the XeF(C) state decays to zero after sufficiently long times, Eq. (2) can be integrated yielding the following expression for the intensity ratio I_B/I_C:

$$\frac{I_B}{I_C} = \frac{\tau_C}{\tau_B}\frac{1}{u}\left(v + \frac{1}{\tau_2}\right) . \tag{12}$$

If one species M_i dominates the mixing reaction between the B and the C levels and the mixing reaction is much faster than the two-body quenching, one obtains approximately

$$\frac{I_B}{I_C} \approx \frac{\tau_C}{\tau_B}\frac{k_{CB}^{M_i}}{k_{BC}^{M_i}} + \frac{\tau_C}{\tau_B}\frac{1}{k_{BC}^{M_i}[M_i]}\frac{1}{\tau_2} . \tag{13}$$

As long as two- and three-body quenching processes of the C state by the species M_i can be neglected compared to the radiative lifetime and quenching processes by other species a plot of I_B/I_C vs $1/[M_i]$ should yield a straight line. When the quenching constants and the radiative lifetimes are known, the slope of this plot yields $k_{BC}^{M_i}$. From the intercept, the ratio of the mixing constants $k_{CB}^{M_i}/k_{BC}^{M_i}$ can be obtained. When the mixing process is rapid enough to establish thermal equilibrium between the two states, the knowledge of $k_{CB}^{M_i}/k_{BC}^{M_i}$ allows a determination of the energy spacing of the B and the C states. In thermal equilibrium the relation

$$\frac{B(t)}{C(t)} = \frac{k_{CB}^{M_i}}{k_{BC}^{M_i}} = \exp(-\Delta E/kT) \tag{14}$$

holds. ΔE is the energy difference between the B and the C states, k the Boltzmann constant, and T the absolute temperature. The ratio of the statistical weights equals unity in this case because both states are doublet states.[17(b),22] A steady state analysis, performed by Brashears and Setser[17(b)] for their experiments yields an equation for I_B/I_C similar to Eq. (13). They measured the ratio $k_{CB}^{M_i}/k_{BC}^{M_i}$ for several cases and found $\Delta E = (680 \pm 40)$ cm^{-1} in good agreement with the experiments of Kilger *et al.*[23] Using some of the results given in Ref. 17(b) Lorents[18(b)] obtains $\Delta E = (630 \pm 23)$ cm^{-1}.

For the integrated Xe_2F fluorescence, an equation can be derived from Eq. (3) that allows, in principle, a determination of the three-body production rate constants of Xe_2F. Using the definitions of the integrated intensities (14), Eq. (3) can be treated in the same manner as Eq. (2) to yield

$$\frac{I_X}{I_C} = \frac{\tau_{eff}}{\tau_X}\left(\tau_B r \frac{I_B}{I_C} + \tau_C s\right) . \tag{15}$$

As I_B/I_C has already been calculated [Eq. (12)], one obtains

$$\frac{I_X}{I_C} = \frac{\tau_{eff}}{\tau_X}\tau_C\left[\frac{r}{u}\left(v + \frac{1}{\tau_2}\right) + s\right] . \tag{16}$$

This fluorescence yield ratio shows a somewhat complicated pressure behavior. In the present case, Eq. (16) can be simplified considerably which will be discussed in Sec. IV C.

The potential surfaces for Xe_2F have been calculated by Huestis.[29(a)] In Fig. 2 the potential surfaces are depicted in the direction where the neutral and ionic states of XeF and Xe are asymptotic states. As in the case of all other rare gas halide trimer molecules, the ground state and lowest excited state potential surfaces are repulsive. For the B and C states, however, an attractive potential is calculated which leads to the formation of the trimer molecule. More recent, calculations[29(b)] take into account the reversed energy ordering of the B and the C state and indicate that the bound $4^2\Gamma$ state comes from the C instead of the B states. The most important difference between the Xe_2F potential surface and other trimer molecules[29] is the potential crossing of the $4^2\Gamma$ state with the $2^2\Gamma$ and $3^2\Gamma$ state near the potential minimum at short internuclear distances. As these states interact, an avoided crossing of these potential surfaces may occur which can lead to a high probability for predissociation for the $4^2\Gamma$ state to XeF(A) and Xe.

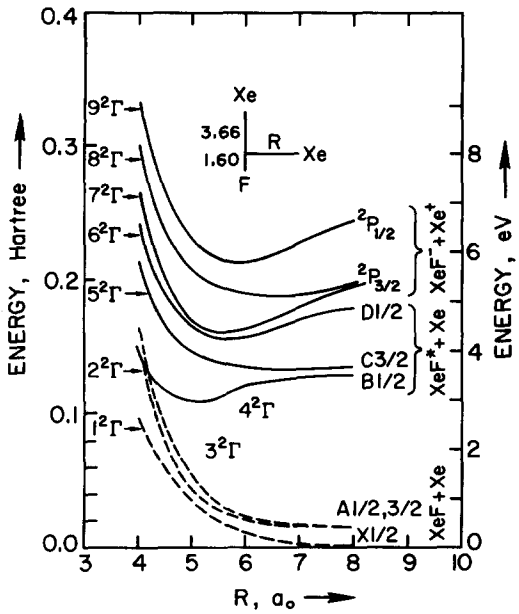

FIG. 2. Potential surfaces of Xe_2F for neutral and ionic states of XeF and Xe as asymptotic states [Ref. 29(a)].

III. EXPERIMENTAL

The experimental setup used in the present investigation is shown in Fig. 3. An intense electron beam is produced by a Physics International Pulsrad 110A generator that excites the gas mixture transversely to the optical axis of a reaction cell. The typical maximum electron current density at the optical axis of the cell was 200 A cm^{-2} as measured by a Faraday cup probe. The maximum electron energy was 1 MeV, and the pulse width (FWHM) of the current pulse was 10 ns. An area of 10 cm × 2 cm was irradiated by the electron beam. Gas mixtures consisting of high purity argon (99.9995%) or neon (99.9996%), xenon (99.995%) and NF_3 (99.5%) were used. With one exception no effect on the observed emission signals that depends upon the number of shots was evident up to about 10 shots. Therefore, every gas mixture was used for several shots (typically about five). Good mixing of the different gas components was achieved by a turbulent flow of the high pressure gas components in the reaction cell.

In order to observe the temporal shape of the fluorescence as well as the fluorescence yield ratios the fluorescence light was guided by beam splitters and mirrors to a photomultiplier in an electrically shielded room and to a Jarrell–Ash spectrometer with a resolution of about 2 nm. The spectrally resolved fluorescence was recorded with an OMA I detection system. The temporal behavior of the fluorescence could also be observed with a vacuum photodiode. The photomultiplier as well as the photodiode were connected to a transient digitizer. The data of both the OMA I and the transient digitizer were processed by a PDP 11/23 minicomputer. The rise time of the photodiode detection system was less than 2 ns and that of the photomultiplier was less than 5 ns. Interference filters and color glass filters were used to define the spectral range of interest.

The temporal shape of the XeF($B-X$) transition around 350 nm was observed through a 350 ± 25 nm interference filter. For the measurement of the XeF($C-A$) transition around 480 nm, a 450 ± 25 nm interference filter was used, and most of the visible and UV fluorescence was suppressed by red filters (Corning 2-60, 2-62) in order to observe the Xe_2F fluorescence. For an accurate measurement of the time dependencies of the XeF($C-A$) and Xe_2F emission care must be taken not to measure in the overlapping wavelength region of the two continua. This was accomplished by means of the 450 nm interference filter and appropriate color glass filters.

In order to analyze Eqs. (3), (12), and (16), a reliable knowledge about the actual intensity ratios is necessary. Therefore, the reflectivity and transmission of all optical elements, as well as the sensitivities of the detectors have been determined and were taken into account. Unfortunately the transmission curve of the spectrometer showed a very steep decrease in the vicinity of 350 nm whereas it was relatively flat between 450 and 700 nm. Therefore, the absolute values of the I_B/I_C ratios may be uncertain by as much as a factor of 2. The I_X/I_C ratios, however, should have an accuracy of better than 20%.

In a second experimental arrangement, the influence of varying electron densities on the XeF–Xe_2F system was studied. A longitudinal pumping scheme similar to that described in Ref. 31 was used. The electron beam had the same energy and pulse width as mentioned above. Only the current density is now controlled by a longitudinal magnetic field. By varying the magnetic field between 0.2 and 1.2 T, the current density was varied from 100 to 1300 A cm^{-2}.

IV. EXPERIMENTAL RESULTS AND DISCUSSION

A. Spectra and vibrational relaxation

The validity of the two-state model which underlies the rate equations (1)–(3) of Sec. II was tested by studying the pressure dependence of the XeF and Xe_2F spectra. Furthermore, the spectral shape of the Xe_2F emission was investigated.

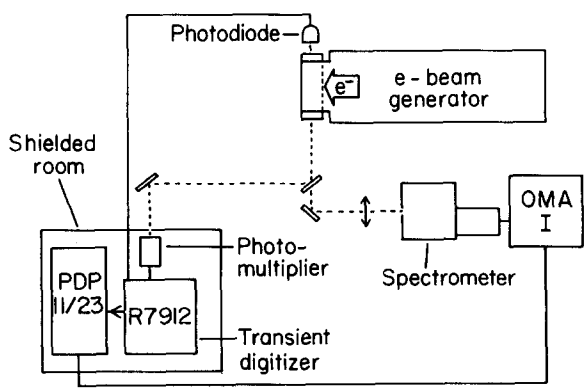

FIG. 3. Experimental setup for transverse electron beam pumping with details for spectral and temporal fluorescence measurements.

Figure 4 shows the fluorescence spectrum of an electron beam-excited Ar–Xe–NF_3 mixture between 250 and 720 nm. The XeF($D-X$)[32] and $B-X$ transitions occur at 265 and 352 nm, respectively. Vibrational structure in these transitions is not resolved due to the limited resolution of the spectrometer. A broad structured continuum is observed that extends from 400 to beyond 720 nm. The short wavelength peak can be assigned to the XeF($C-A$) emission,[11(a),17(a),21] whereas the long wavelength peak is due to Xe_2F.[30] At argon pressures of 6 atm, the vibrational relaxation in the XeF(B) and XeF(C) states occurs very rapidly.[17(b)] The spectral shape of the $C-A$ transition is therefore independent of the pressure in this region. The shape of the Xe_2F transition can thus be obtained by subtracting the XeF($C-A$) transition from the continuum. In this way, the maximum of the Xe_2F emission was determined to lie at (614 ± 5) nm with a spectral bandwidth (FWHM) of (125 ± 5) nm. These data are in good agreement with the preliminary results reported previously[30] which were obtained from uncorrected spectra. The potential surface calculations for Xe_2F[29] yield a value between 615 and 808 nm for the Xe_2F emission wavelength. The lower bound of these calculations is in agreement with the experimental observations.

Similar spectra to those obtained in Ar–Xe–NF_3 mixtures were also observed for Ne–Xe–NF_3 mixtures when the Ne pressure was above 3 atm. However, quantitative measurements with Ne as a buffer gas were complicated by intense emissions from many neon lines that lie between 500 and 700 nm.

The vibrational distribution in the XeF(C) state can be qualitatively studied by the observation of the spectral width of the $C-A$ transition. In Fig. 5, the spectral shape of the XeF($C-A$) transition is shown for three different argon pressures in a Ar–Xe–NF_3 gas mixture. For very low argon pressures (20 Torr), a FWHM of as much as 100 nm is observed. When the argon pressure is raised to about 100 Torr, the width decreases considerably to about 78 nm. Further narrowing of the spectrum has been observed for argon pressures up to 3 atm. For higher pressures the shape of the spectrum remained constant up to the highest argon pressure used in the present experiments of 8 atm.

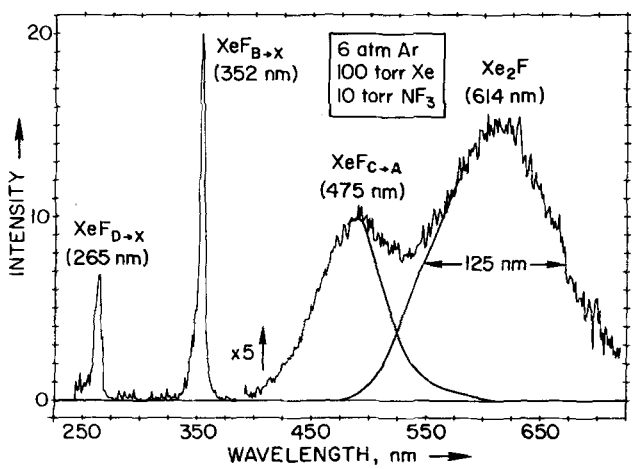

FIG. 4. Spectrum of an electron beam excited Ar–Xe–NF_3 mixture between 250 and 720 nm. The spectra are corrected for the wavelength dependent sensitivity of all optical elements used in the experiment. The solid lines indicate the spectral shape of the XeF($C-A$) transition and the Xe_2F emission.

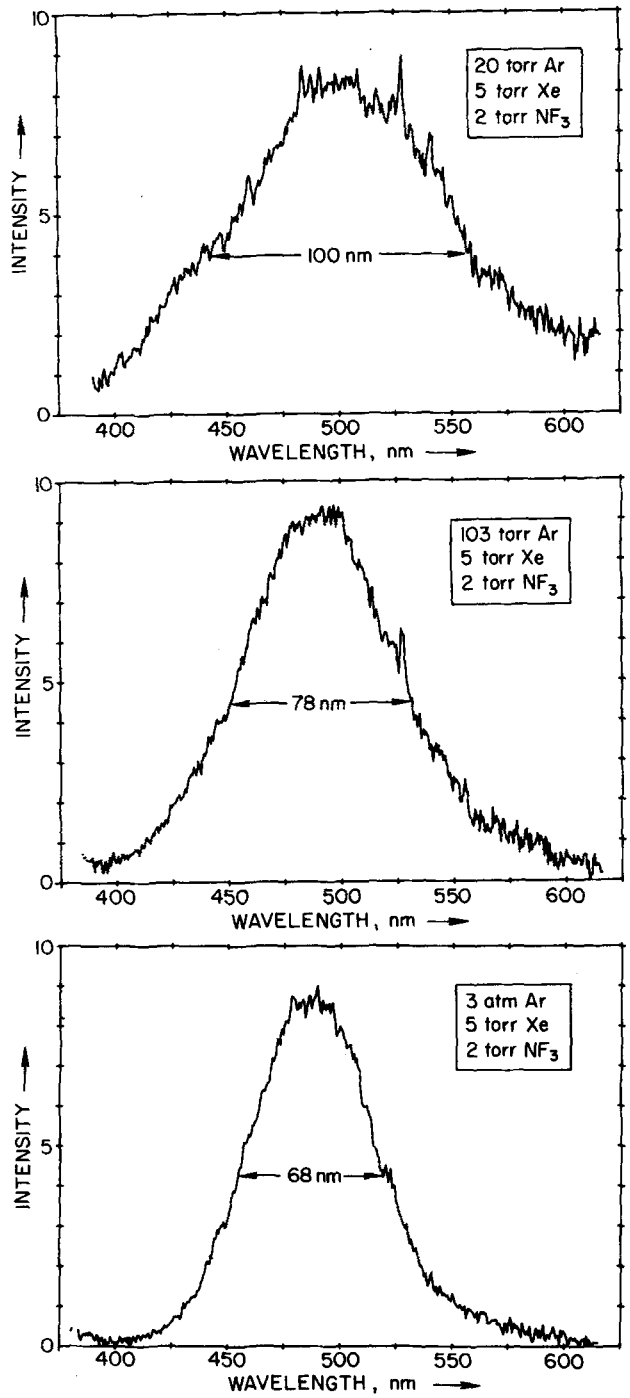

FIG. 5. Shape of the XeF($C-A$) transition for three different argon pressures.

Similar observations were made for the XeF($B-X$) transition, using the spectrometer in second order. Spectral narrowing was nearly complete at argon pressures of the order of 100 Torr, but a slight change in spectral shape with increasing pressure was observed up to pressures of about 2 atm. As far as the $B-X$ transi-

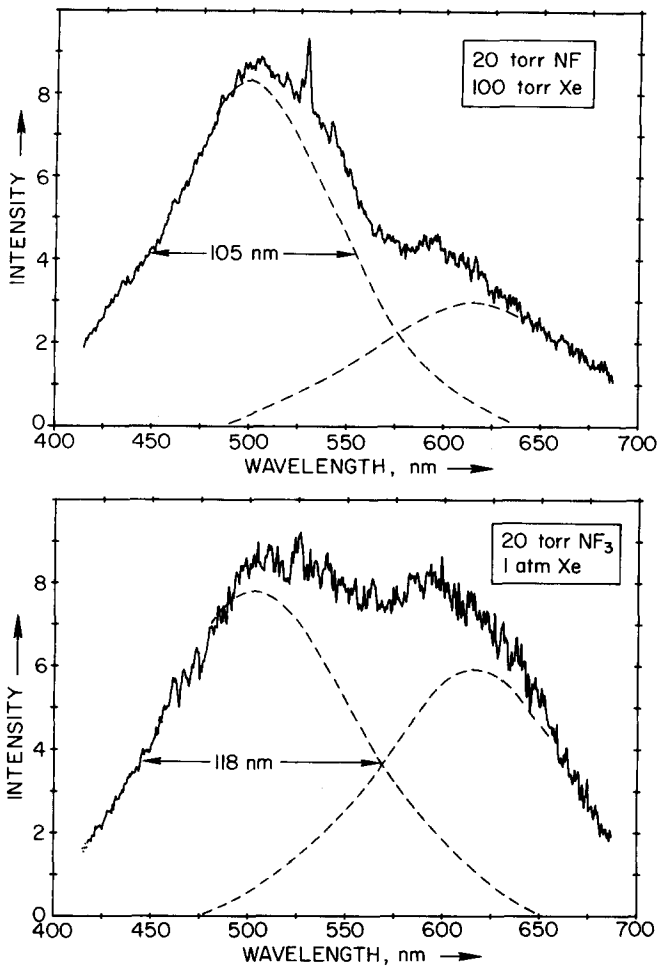

FIG. 6. XeF($C \rightarrow A$) transition and Xe_2F transition for 100 Torr Xe, and 1 atm Xe. The dashed lines indicate the XeF($C \rightarrow A$) and the Xe_2F emission.

tion is concerned, these results are in agreement with results by Brashears and Setser.[17(b)] They observed a 300 K Boltzmann vibrational distribution for the B state for argon pressures above 2000 Torr. A 300 K Boltzmann distribution for the C state was already obtained for about 400 Torr of argon. This is considerably lower than the value of about 3 atm observed in the present investigation. A possible reason for this discrepancy may be due to the fact that further narrowing of the $C \rightarrow A$ spectrum beyond about 100 Torr of argon is small and therefore difficult to measure. As the potential curve of the B state is embedded in the C state potential curve,[18(b),22] collisional mixing between both states should also occur for higher vibrational levels. Therefore, it seems unlikely that the buffer gas pressures which are necessary to achieve a 300 K Boltzmann distribution are very different for the two states. From the observation that with about 100 Torr of argon a considerable vibrational relaxation in the two states is achieved, a rough order of magnitude estimate of an average vibrational relaxation rate constant for both states can be obtained, yielding a value of the order of 10^{-11} $cm^3 s^{-1}$.

For a $Xe-NF_3$ mixture a pressure behavior of the fluorescence that differs from that of $Ar-Xe-NF_3$ mixtures is observed. Figure 6 shows that with increasing xenon pressure no spectral narrowing of the $C \rightarrow A$ transition is obtained. The Xe_2F formation which can be suppressed in the case of $Ar-Xe-NF_3$ mixtures by choosing a low xenon partial pressure is inherent for $Xe-NF_3$ mixtures at high xenon pressures. The determination of the spectral bandwidth of the $C \rightarrow A$ transition is somewhat uncertain because an assumption about the spectral shape of the Xe_2F transition has to be made. However, no vibrational relaxation in the XeF(C) state occurs with increasing xenon pressure. The same observation was made for the $B \rightarrow X$ transition.

Since no vibrational relaxation in the B and the C state occurs during its decay in $Xe-NF_3$ mixtures, the decay of both states must be much faster than the process of vibrational relaxation by collisions with xenon atoms. Assuming that the vibrational energy transfer probability for xenon is of the same order of magnitude as that for argon, a high two- or three-body quenching rate of XeF(B, C) by Xe is required in order to describe the observed behavior of $Xe-NF_3$ mixtures.

In $Xe-NF_3$ mixtures a shift of the maximum of the $C \rightarrow A$ transition from (480 ± 5) nm (Fig. 5) to (500 ± 10) nm (Fig. 6) is observed. This shift, although its actual magnitude is somewhat uncertain, seems to be virtually independent of the xenon pressure. Such a shift in the maximum of the $C \rightarrow A$ transition has also been observed by Rokni *et al.*[14(a)] It was tentatively assigned to the formation of ArXeF* and NeXeF*. Further attempts to observe ArXeF* and NeXeF* have failed,[24] and it was emphasized by Brashears *et al.*[24] that this may be due to the low binding energy of ArXe* and NeXe*[34] causing unstable trimer molecules involving these species. As the experiments of Rokni *et al.*[14(a)] were performed at argon pressures where the vibrational distribution is close to a 300 K Boltzmann distribution, their observed pressure dependent shifts of the maximum of the $C \rightarrow A$ transition are probably not due to an incomplete vibrational relaxation in the C level.[17(b)] However, it is likely that they are, in fact, caused by the formation of Xe_2F. This explanation would describe the observed shift of their emission maxima to longer wavelengths with increasing argon pressure due to an enhanced Xe_2F formation.

Due to the fact that in $Xe-NF_3$ mixtures no vibrational relaxation of the B and the C states can be achieved, the determination of rate constants from measurements in $Xe-NF_3$ mixtures is severely restricted. All rate constants which are obtained from those mixtures are in fact averages over a widely unknown vibrational distribution. In an $Ar-Xe-NF_3$ mixture, however, a 300 K vibrational distribution is achieved for several atmospheres of argon. The energy spacing of the lower vibrational levels of the B state is 308 cm^{-1}.[33] Hence, mainly the lowest vibrational levels are populated at 300 K, and the measured rate constants correspond to the lowest vibrational levels of the B and the C states.

B. Two- and three-body quenching of XeF(B, C)

In studying the quenching processes of XeF(B, C), the fluorescence yield ratios as well as the temporal de-

pendencies of the emitting species have been investigated. Figure 7 shows the temporal behavior of the XeF(B), the XeF(C), and the Xe_2F fluorescence as well as the electron beam pulse as measured by a Faraday cup probe. The maximum of the XeF(B) emission occurs at the end of the electron beam pulse indicating direct production of the B state primarily by fast ionic reactions. The C state emission appears somewhat delayed. This supports the assumption made in solving Eqs. (1) and (2) that direct C state production is negligibly small ($P_c = 0$). The C state is populated via collisions from the B state as expressed in Eqs. (6) and (8). The decay frequencies were measured by determining the slope of the logarithm of the decaying part of the pulses over two to four e foldings. The onset of the Xe_2F pulse is on the same time scale as the width of the XeF pulses which is to be expected when Xe_2F is formed from XeF by fast three-body quenching processes. Xe_2F typically decays with a much slower decay frequency than the XeF species indicating a comparatively long radiative lifetime of Xe_2F. At low xenon pressures (< 20 Torr) an intense red emission mainly due to the $4p'-4s$ transition in argon at 695.5 nm[35] was superimposed on the onset of the XeF_2 emission. The temporal shape of this argon emission was measured in argon and Ar/NF_3 mixtures, and could be subtracted from the XeF_2 emission.

In order to determine the two- and three-body quenching rate constants for the B and the C states, the decay frequencies for both states were measured as a function of the partial pressures of Ar, Xe, and NF_3. No efforts were made to determine the radiative lifetimes of both states because reliable values for the radiative lifetimes are already available. The values of $\tau_B = 13.2$ ns and $\tau_C = 101$ ns recently obtained by Lorents *et al.*[18(b)] were used in the present work. To ensure good vibrational relaxation in the B and the C state (see Sec. III) the experiments concerning Xe and NF_3 were performed in a 6 atm Ar atmosphere.

In Fig. 8, the decay frequencies for the B and the C states emissions are shown as functions of the NF_3 partial pressure yielding the same straight line for both states within the experimental uncertainties. According to the discussion in Sec. III, this means that the collisional mixing is much faster than the decay processes for both states. This can be verified by calculating $u + v$ using Lorents' results[18(b)] yielding $u + v \approx 2.3 \times 10^9\ s^{-1}$. Thermal equilibrium between both states is thus obtained on a ns time scale. This is much faster than the decay which occurs with a typical time of about 30 ns (Fig. 7). The term $k_{BC}^{Ar}[Ar]$ is by far the dominating term in u. Therefore, Eq. (10) can be used to analyze the quenching by NF_3 yielding for the slope σ_{NF_3} of the straight line in Fig. 8:

$$\sigma_{NF_3} = \frac{k_{CB}^{Ar}}{k_{BC}^{Ar} + k_{CB}^{Ar}} k_B^{NF_3} + \frac{k_{BC}^{Ar}}{k_{BC}^{Ar} + k_{CB}^{Ar}} k_C^{NF_3}. \quad (17)$$

This gives an example of how a coupled rate constant for XeF* can be obtained from the rate constants of the individual states in the case of complete vibrational relaxation and thermal equilibrium. With the energy spacing between the B and the C state given in Sec. II, a ratio $k_{CB}^{Ar}/k_{BC}^{Ar} = 0.044$ using Eq. (14) is obtained. It was observed by Brashears and Setser[17(b)] that the quenching for both states by a certain species is approximately the same. The first term in Eq. (17) is, therefore, only about 4% of the second term and can be neglected. This yields a value of $k_C^{NF_3} = (1.5 \pm 0.2) \times 10^{-11}\ cm^3\ s^{-1}$. In the case of complete vibrational relaxation and thermal equilibrium, this is essentially the quenching of XeF*. For the intersection θ_{NF_3} (Fig. 8), we obtain

$$\theta_{NF_3} = \frac{k_{BC}^{Ar}}{k_{CB}^{Ar} + k_{BC}^{Ar}} \left[\frac{1}{\tau_C} + (k_C^{Xe} + k_C^{Xe\cdot Ar}[Ar])[Xe] + k_C^{Ar}[Ar] \right]. \quad (18)$$

Here again the term proportional to k_{CB}^{Ar} was neglected. From the three-body quenching terms of τ_2^{-1}, only the term $k_C^{Xe\cdot Ar}[Ar][Xe]$ is of importance because of the relatively high argon pressure. The potentially larger term $k_C^{Ar\cdot Ar}[Ar]^2$ can be neglected because the three-body quenching rate of XeF(C) by two Ar is vanishingly small (see below). All the other possible three-body quenching

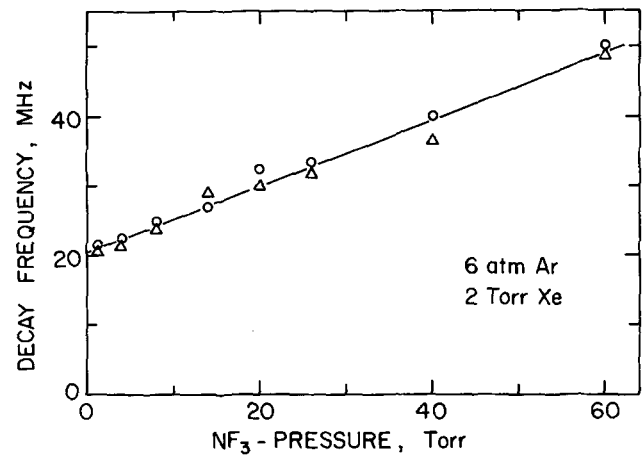

FIG. 8. XeF(B) and XeF(C) decay frequency as a function of the NF_3 pressure. The circles (○) denote the B state, the triangles (△) correspond to the C state.

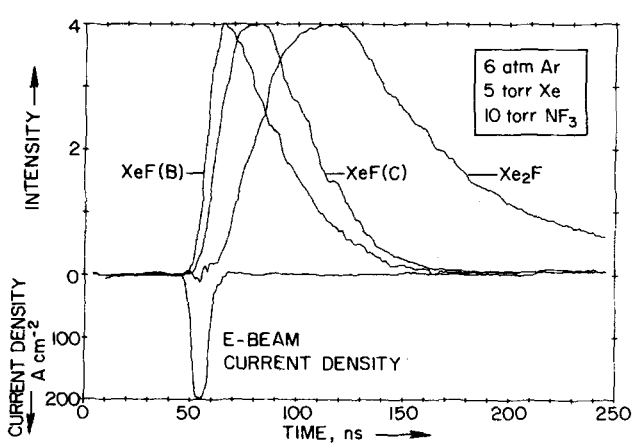

FIG. 7. Temporal dependence of the e-beam current, the XeF(B), XeF(C, and Xe_2F emission. The fluorescence signals have been normalized to the same maximum value. An emission from red argon lines has been subtracted from the Xe_2F fluorescence pulse.

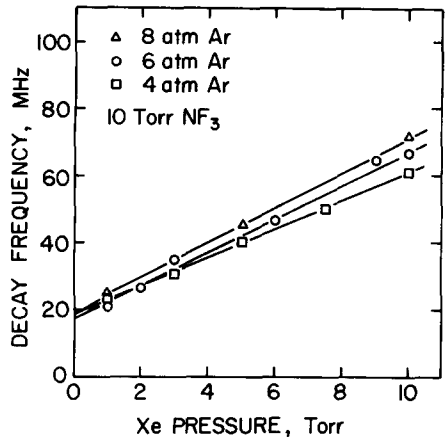

FIG. 9. Decay frequency of the XeF(C) fluorescence as a function of the xenon pressure for three different argon pressures.

terms can be neglected.

$k_C^{Xe} + k_C^{XeAr}[Ar]$ can be obtained from Fig. 9. In this figure, the decay frequency of XeF(C) vs the xenon pressure is shown for three different argon pressures. In each case the argon pressure is high enough to ensure rapid collisional mixing and vibrational relaxation. The slopes are slightly different for different argon pressures which is to be expected if the three-body quenching of the C state by argon and xenon is of importance. In the same approximation as for Eq. (17), the slopes of Fig. 9 are obtained from Eq. (10)

$$\sigma_{Xe} = \frac{k_{BC}^{Ar}}{k_{BC}^{Ar} + k_{CB}^{Ar}} (k_C^{Xe} + k_C^{XeAr}[Ar]) . \quad (19)$$

This yields $k_C^{Xe} = 1.1\times10^{-10}$ cm^3 s^{-1} and $k_C^{XeAr} = 3.4\times10^{-31}$ cm^6 s^{-1}. From the intersection of zero xenon pressure (Fig. 9), the radiative lifetime of the XeF(C) state can be determined to be (97 ± 5) ns.

The two-body quenching of XeF(C) by xenon can also be obtained from the fluorescence yield ratios in Fig. 10. From the values for the collisional mixing rate constants for argon and xenon given in Ref. 18 the collisional mixing by 6 atm of argon dominates the xenon mixing even at 200 Torr xenon pressure. Therefore, Eq. (13) describes the xenon pressure dependence of I_B/I_C. A straight line with an intersection at

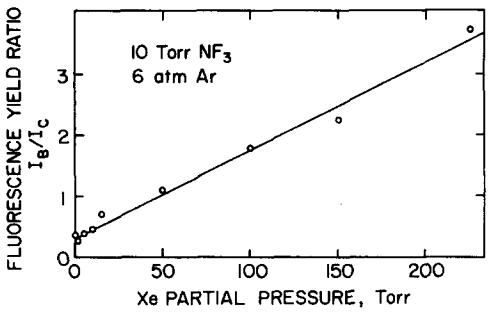

FIG. 10. Xenon pressure dependence of the fluorescence yield ratio I_B/I_C.

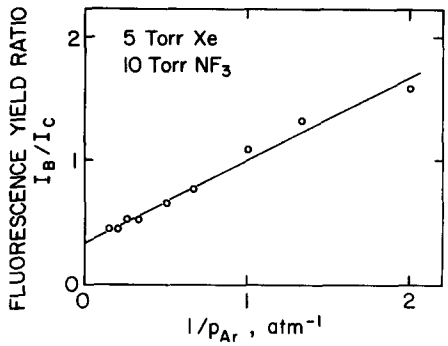

FIG. 11. Fluorescence yield ratio I_B/I_C as a function of the inverse argon pressure p_{Ar}^{-1}. The intersection at $p_{Ar}^{-1} = 0$ has been scaled to 0.33.

$\tau_C k_{CB}^{Ar}/\tau_B k_{BC}^{Ar} = 0.33$ and a slope of

$$\Sigma_{Xe} = \frac{\tau_C}{\tau_B} \frac{1}{k_{BC}^{Ar}[Ar]} (k_C^{Xe} + k_C^{XeAr}[Ar]) \quad (20)$$

is expected from Eq. (13). The experimental results agree well with this prediction (Fig. 10). It was mentioned earlier that the absolute ratios of I_B/I_C may be uncertain by as much as a factor of 2 whereas the relative accuracy of the experimental points should be about 10%. As the intersection depends only on well-known quantities as the radiative lifetimes and the energy difference between the B and the C states [Eq. (14)], the experimental values were scaled up from an intersection at 0.25 to an intersection at 0.33. Then from the slope [Eq. (20)] and with the knowledge of $k_{BC}^{Ar} = 1.5\times10^{-11}$ cm^3 s^{-1} (see below) a value of

$$k_C^{Xe} + k_C^{XeAr}[Ar] = 1.8\times10^{-10} \text{ cm}^3 \text{ s}^{-1}$$

is obtained. With $k_C^{XeAr} = 3.4\times10^{-31}$ cm^6 s^{-1} this yields $k_C^{Xe} = 1.3\times10^{-10}$ cm^3 s^{-1} which is in agreement with the value obtained from the analysis of the decay times. The now specified values for k_C^{Xe} and k_C^{XeAr} allow an estimate of the two-body quenching constant k_C^{Ar} from Eq. (18). This yields $k_C^{Ar} < 1\times10^{-14}$ cm^3 s^{-1} as an upper limit. The value of $\tau_C k_{CB}^{Ar}/\tau_B k_{BC}^{Ar} = 0.25$ with an estimated error of about a factor of 2 would lead to an energy difference between the B and the C states of $\Delta E = (720 \pm 140)$ cm^{-1} which is in agreement with the results obtained by others[17(b),18(b),23] but less accurate.

In order to justify the assumption that argon is the dominant collisional mixer in Ar/Xe/NF_3 mixtures with several atmospheres of argon and xenon and NF_3 pressures of the order of several Torrs the fluorescence yield ratio I_B/I_C as a function of $1/p_{Ar}$ (p_{Ar} denotes the argon pressure) is shown in Fig. 11. If argon is the dominant collisional mixer, Eq. (13) predicts a straight line for the experimental values in Fig. 11, which is observed for $1/P_{Ar}$ less than about 2 atm^{-1}. For lower argon pressures, some deviations from this behavior were observed that may be due to a lack of vibrational relaxation in both states as well as interference of the argon mixing by that of xenon and NF_3. As τ_2^{-1} is now known with sufficient accuracy k_{BC}^{Ar} can be determined from the slope of Fig. 11. The intersection is again adjusted to 0.33. This yields the result $k_{BC}^{Ar} = (1.5 \pm 0.3) \times10^{-11}$ cm^3 s^{-1}.

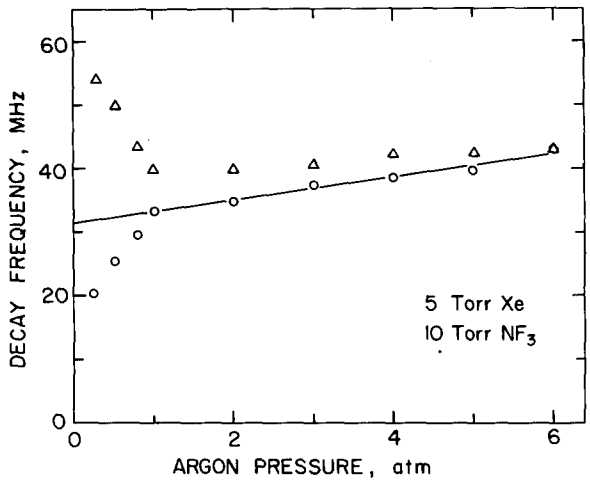

FIG. 12. Decay frequencies of the B and the C states as function of the argon pressure. The circles (O) denote the C state, the triangles (Δ) correspond to the B state.

The three-body quenching of XeF(C) by xenon and argon was determined from a slight difference in the slopes for different argon pressures in Fig. 9. A more reliable result can be obtained when the decay frequency of XeF(B, C) as a function of the argon pressure is investigated (Fig. 12). This figure shows the near coincidence of the decay times of the B and the C states for argon pressures of more than about 1 atm, which is expected when both states are immediately in thermal equilibrium. Below 1 atm argon pressure, the decoupling of the two states can be observed. The time to establish thermal equilibrium between both states becomes measurable, and the decay of the B state consists then of two exponentials. The lower of the two decay frequencies coincides with the decay of the C state as predicted by Eqs. (5) and (6). For the C state, only one decay frequency was observed.

For pressures above an atmosphere, the collisional mixing by argon is sufficiently fast in order to use Eq. (10) for the analysis of the decay times of XeF(C). Neglecting again the term proportional to k_{CB} in the slope σ_{Ar} of the solid line σ_{Ar} of Fig. 12 yields [Eq. (10)]

$$\sigma_{Ar} = \frac{k_{BC}^{Ar}}{k_{BC}^{Ar} + k_{CB}^{Ar}} \left(k_C^{Xe*Ar}[Xe] + k_C^{Ar}\right) . \qquad (21)$$

With the value for k_C^{Ar} estimated above, $k_C^{ArXe*} = (4.3 \pm 0.3) \times 10^{-31}$ cm^6 s^{-1} is obtained from Eq. (21) and Fig. 12. The error in k_C^{ArXe*} arises from the uncertainty in k_C^{Ar}. The value is in good agreement with $k_C^{ArXe*} = 3.4 \times 10^{-31}$ cm^6 s^{-1} obtained from Fig. 9, and a mean value of $k_C^{ArXe*} = (3.9 \pm 0.5) \times 10^{-31}$ cm^6 s^{-1} is obtained. The intersection at zero argon pressure contains the two-body quenching of XeF(C) by xenon and other constants. From this $k_C^{Xe*} = 1.2 \times 10^{-10}$ cm^3 s^{-1} can be determined which is in excellent agreement with the previous values for this rate constant. The two-body quenching constant of XeF(C) by xenon has now been determined from three independent measurements yielding an average value of $k_C^{Xe*} = (1.2 \pm 0.3) \times 10^{-10}$ cm^3 s^{-1}.

From the dependence of the maximum of the temporal pulses of XeF(B, C) on the argon pressure, an estimate for the three-body quenching constants of the B and the C states by argon can be obtained. Upper limits of 3×10^{-33} cm^6 s^{-1} for k_B^{ArAr} and k_C^{ArAr} have been determined.

The two- and three-body quenching rate constants are all listed in Table I. The errors contain statistical errors as well as estimated systematic errors due mainly to the gas pressure measurement and an uncertainty in the exact time calibration of the transient digitizer. The two-body rate constants obtained in this work are then compared to those obtained in Refs. 17 and 18 because only these investigations take into account the right energy ordering of the XeF states and collisional mixing.

As far as a comparison is possible, there is excellent agreement between the rate constants obtained by Black *et al.*[18] and those obtained in this work. Only the value of the present experiment for k_C^{Xe*} is somewhat lower than that of Ref. 18. When three-body quenching of the C state by xenon and argon is neglected in the present analysis, a value of $(1.8 \pm 0.3) \times 10^{-10}$ cm^3 s^{-1} for k_C^{Xe*} would be obtained which would then be in agreement with the rate constant determined in Ref. 18. This might be explained by the fact that the experiments of Ref. 17 were performed in a pure xenon atmosphere where no vibrational relaxation occurs. Therefore, this rate constant corresponds to a totally different vibrational temperature than those obtained in the present investigation.

A value of more than 10^{-10} cm^3 s^{-1} is a very high rate coefficient for a two-body quenching reaction of neutral collision partners involving a rare gas. This can, however, be qualitatively understood when the potential describing a XeF(C)–Xe collision is considered (Fig. 2). When the potential crossing lies at a lower energy than the energy of the asymptotic states, the crossing of the attractive $4^2\Gamma$ potential with the repulsive potentials is passed in every two-body collision of XeF(C) with Xe with the possibility of predissociation of the short living Xe_2F complex into XeF(A) and Xe. As XeF(B) has a different potential in the collision with Xe, a much lower two-body quenching constant for XeF(B) by xenon is expected. The high quenching constant for XeF(C) by xenon has also the right order of magnitude in order to explain the lack of vibrational relaxation in Xe–NF_3 mixtures. As the same crossing of potential curves probably occurs also for highly vibrational excited XeF molecules, the predissociation probability may be higher than the probability for a V–T energy transfer. XeF will therefore decay before vibrational relaxation is achieved.

The value for $k_C^{NF_3}$ of Ref. 17 agrees well with the value obtained in the present experiment, but the values for k_C^{Ar} and k_{BC}^{Ar} differ. In the case of k_C^{Ar}, this could be due to the neglecting of three-body quenching effects in Ref. 17(b). In this case, a reaction of the XeF(B, C) with argon and XeF_2 might be possible which would yield qualitatively the observed pressure behavior of I_B/I_C [17(b)] but with a higher "two-body" rate coefficient. The discrepancy of k_{BC}^{Ar} between Ref. 18 and the present work and Ref. 17(b) is only small and may be due to experimental errors in either work.

TABLE I. Kinetic reactions for XeF and Xe_2F.

Reaction		This work	Black *et al.* (Ref. 18)	Brashears and Setser (Ref. 17)	Footnote
(1) $XeF(C) + NF_3 \rightarrow$ products	$k_C^{NF_3}$	$(1.5 \pm 0.3) \times 10^{-11}$ cm^3/s		$(1.4 \pm 0.6) \times 10^{-11}$ cm^3/s	
(2) $XeF(C) + Ar \rightarrow$ products	k_C^{Ar}	$< 1 \times 10^{-14}$ cm^3/s	$(7 \pm 7) \times 10^{-15}$ cm^3/s	$(5 \pm 2) \times 10^{-14}$ cm^3/s	
(3) $XeF(C) + Xe \rightarrow$ products	k_C^{Xe}	$(1.2 \pm 0.3) \times 10^{-10}$ cm^3/s	1.9×10^{-10} cm^3/s	$(1.8 \pm 0.5) \times 10^{-11}$ cm^3/s	a
(4) $XeF(B) + Ar \rightarrow XeF(C) + Ar$	k_{BC}^{Ar}	$(1.5 \pm 0.3) \times 10^{-11}$ cm^3/s	$(1.4 \pm 0.2) \times 10^{-11}$ cm^3/s	$(0.86 \pm 0.11) \times 10^{-11}$ cm^3/s	
(5) $XeF(B) + e^- \rightarrow XeF(C) + e^-$	k_{BC}^{e}	negligible			b
(6) $XeF(C) \rightarrow Xe + F + h\nu$	τ_C	(97 ± 5) ns	(101 ± 2) ns		c
(7) $XeF(C) + Ar + Xe \rightarrow$ products	k_C^{XeAr}	$(3.9 \pm 0.5) \times 10^{-31}$ cm^3/s			d, g
(8) $XeF(B) + 2Ar \rightarrow$ products	k_B^{ArAr}	$< 3 \times 10^{-33}$ cm^6/s			e
(9) $XeF(C) + 2Ar \rightarrow$ products	k_C^{ArAr}	$< 3 \times 10^{-33}$ cm^6/s			
(10) $XeF(C) + 2Xe \rightarrow$ products	k_C^{XeXe}	$(4 \pm 1) \times 10^{-32}$ cm^6/s		$< 3 \times 10^{-31}$ cm^6/s	f
(11) $XeF(C) + 2Xe \rightarrow Xe_2F + Xe$	k_{CP}^{XeXe}	$(2.7 \pm 0.6) \times 10^{-32}$ cm^6/s			f
(12) $XeF(C) + Xe + Ar \rightarrow Xe_2F + Ar$	k_{CP}^{XeAr}	$(1.1 \pm 0.3) \times 10^{-31}$ cm^6/s			
(13) $Xe_2F + NF_3 \rightarrow$ products	$k_X^{NF_3}$	$(7.8 \pm 1.2) \times 10^{-13}$ cm^3/s			
(14) $Xe_2F + Xe \rightarrow$ products	k_X^{Xe}	$(1.0 \pm 0.2) \times 10^{-13}$ cm^3/s			
(15) $Xe_2F + Ar \rightarrow$ products	k_X^{Ar}	$(2.8 \pm 0.9) \times 10^{-14}$ cm^3/s			
(16) $Xe_2F \rightarrow 2Xe + F + h\nu$	τ_X	(152^{+19}_{-10}) ns			

[a]Value of (Ref. 17) measured for a high, but unknown vibrational temperature; other values for the quenching of XeF* in Refs. 14(b), 15, and 21.
[b]In the afterglow of short pulse e-beam excitation.
[c]See also [Refs. 13(b), 19, and 20].
[d]$(3 \pm 1.5) \times 10^{-31}$ cm^6 s^{-1} [Ref. 14(d)].
[e]$(1.5 \pm 0.5) \times 10^{-32}$ cm^6 s^{-1} [Ref. 14(d)].
[f]Value of this work measured for a high, unknown vibrational temperature; other values for three-body quenching of XeF* in Refs. 14(b) and 15.
[g]3×10^{-31} cm^6 s^{-1} (Ref. 43).

Three-body quenching of XeF(C) by argon and xenon is reported here for the first time. A quenching rate of XeF* by xenon and argon has been measured by Rokni *et al.*[14(d)] to be $(3 \pm 1.5) \times 10^{-31}$ cm^6 s^{-1}. This has to be assigned to some linear combination of k_B^{ArXe} and k_C^{ArXe} depending on the collisional mixing process in this experiment. This rate constant can also be compared to the rate coefficieint for a similar trimer system Xe_2Br*[36] where about the same value has been measured. Rokni *et al.*[14(d)] have also measured the three-body quenching of XeF by two Ar and determined a value of 1.5×10^{-32} cm^6 s^{-1} for this process, which is about five times higher than the upper limit for this process determined in this work. The rate constant of Ref. 14(d) would yield a decay time of about 3 ns for the XeF(B, C) temporal pulses at 6 atm argon which was not observed in the present experiments (Fig. 7).

In order to investigate the contribution of electrons to the collisional mixing process between XeF(B) and XeF(C), the temporal behavior of the XeF fluorescence pulses as function of the exciting current density was studied at low argon pressures. The experimental results show that the decay frequencies for the B and the C states increase slightly up to a maximum current density of about 700 A cm^{-2} and remain approximately constant up to about 1300 A cm^{-2}. No influence in the difference in the decay frequencies of both states was observed. The slight increase of the decay times with increasing current density represents the quenching of the XeF states by super-elastic collisions with electrons. Its influence on the value of the decay frequencies can be estimated to be less than 5% for a current density of 200 A cm^{-2}.

In a second experiment, the maximum current density remained constant at about 600 A cm^{-2}, and the electron density was influenced by the addition of SF_6 to the gas mixture. SF_6 is known to possess a large electron capture cross section[37] and was used previously to reduce electron densities in electron beam pumped media.[38–40] The collisional mixing and quenching rate constants of SF_6 for XeF(B, C) are small enough not to influence the XeF kinetic for SF_6 partial pressures of several Torr.[17(b)] The addition of several Torr SF_6 caused no measurable change in the temporal behavior of XeF(B) and XeF(C) although it should have influenced the electron density severely.[37]

From both experiments it can be concluded that electrons in the afterglow of the electron beam excitation pulse have no measurable influence on the collisional mixing process of the B and the C states. This result is in agreement with that obtained by Finn *et al.*,[41] who

also found no influence of the electron density in the mixing process of XeF(B) and XeF(C) when long pulse, low current density electron beam excitation was used.

In the absence of collisional mixing by electrons, it is possible to obtain the three-body quenching constant for XeF(C) by two Xe from the analysis given by Walter *et al.*[30] When collisional mixing by neutrals instead of electrons is assumed, a value of $k_C^{XeXe} = 4\times10^{-32}$ cm^6 s^{-1} can be obtained. This rate coefficient corresponds to a high, unknown vibrational temperature of XeF(C) as outlined in Sec. III. It is in agreement with an upper limit of 3×10^{-31} cm^6 s^{-1} given by Brashears and Setser.[17(b)] The value for k_C^{XeXe} is about an order of magnitude lower than for k_C^{ArXe} or the comparable processes of the quenching of XeBr* by two Xe[36] and ArF* by two Ar.[42] This might also be due to the absence of vibrational relaxation in Xe–NF_3 mixtures. The binding energy of Xe_2F relative to XeF(C) and Xe is only about 0.5 eV (Fig. 2). For a highly vibrationally excited XeF(C) molecule, it might therefore be impossible to form Xe_2F because its vibrational energy is higher than the binding energy of Xe_2F, leading to an immediate dissociation of Xe_2F into XeF(C) and xenon. This would cause a smaller three-body quenching constant of XeF(C) by two Xe than in cases where vibrational relaxation has been achieved.

C. Formation and quenching of Xe_2F

In Fig. 13, the temporal dependence of a Xe_2F pulse and two numerical solutions of Eq. (3) are shown. The experimentally determined fluorescence pulses of XeF(B, C) (Fig. 7) were used to solve Eq. (3). For the calculated curve denoted by B, it was assumed that Xe_2F is produced only from the XeF(B) state ($s = 0$), whereas, for the curve denoted by C, a Xe_2F production only from the XeF(C) state was assumed ($r = 0$). When r and s were both chosen unequal zero, and of about the same magnitude, the onset of the calculated curve always showed deviations from the measured pulse which disappeared when s was much greater than r. This calculation demonstrates that XeF(C) is the precursor of Xe_2F. A rate constant of $k_{CP}^{XeAr} = 0.8\times10^{-31}$ cm^6 s^{-1} was extracted from several fits like that in Fig. 13. The result that Xe_2F is produced from the XeF(C) state corroborates recent calculations[29(b)] that show that the bound $4^2\Gamma$ state of Xe_2F correlates to the XeF(C) state (Fig. 2).

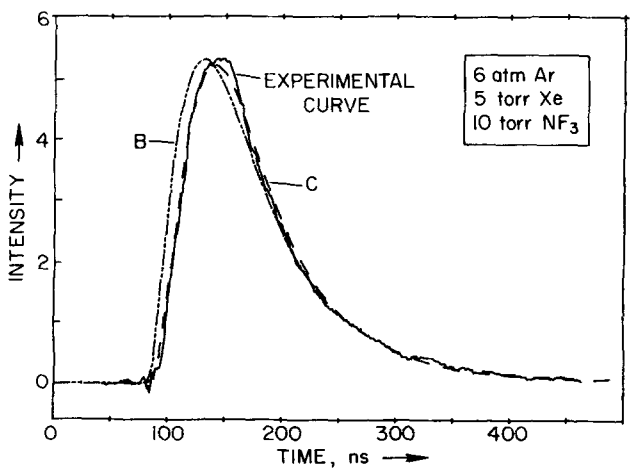

FIG. 13. Temporal dependence of the Xe_2F fluorescence pulse. The dashed curves denoted by B and C are solutions of Eq. (3) when only the B or C state were considered as precursors for Xe_2F.

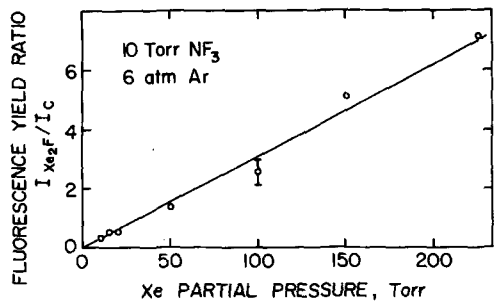

FIG. 14. Fluorescence yield ratio I_{Xe_2F}/I_C as a function of the xenon partial pressure in an Ar–Xe–NF_3 mixture.

With this result the determination of rate constants from the fluorescence yield ratios is simplified considerably. Equation (16) is reduced to

$$\frac{I_X}{I_C} = \frac{\tau_C}{\tau_X}\cdot\tau_{eff}\cdot s\,. \tag{22}$$

For mixtures with several atmospheres of argon and several Torr xenon, the term in s which is proportional to [Xe][Ar] dominates. When the small two-body quenching of Xe_2F by xenon and argon is neglected (see below), $I_X/I_C \sim$ [Ar][Xe] is expected. In Fig. 14, I_X/I_C is shown as a function of the xenon pressure. It shows the expected linear dependence on the xenon pressure. From Eq. (22) and Fig. 14, the three-body production rate k_{CP}^{XeAr} of Xe_2F can be calculated yielding $k_{CP}^{Ar} = 1.1\times10^{-31}$ cm^6 s^{-1}. This is in reasonable agreement with the value obtained from temporal measurements (Fig. 13) and a value of $k_{CP}^{ArXe} = (1.0\pm0.2)\times10^{-31}$ cm^6 s^{-1} is established.

In the case of Xe–NF_3 mixtures, Eq. (22) predicts $I_X/I_C \sim$ [Xe]^2. This is also observed in the experiment which is shown in Fig. 15. I_X/I_C as a function of the square of the xenon pressure p_{Xe} yields a straight line. From Fig. 15 and Eq. (22), a Xe_2F production rate constant of k_{CP}^{XeXe} of $(2.7\pm0.6)\times10^{-32}$ cm^6 s^{-1} can be deter-

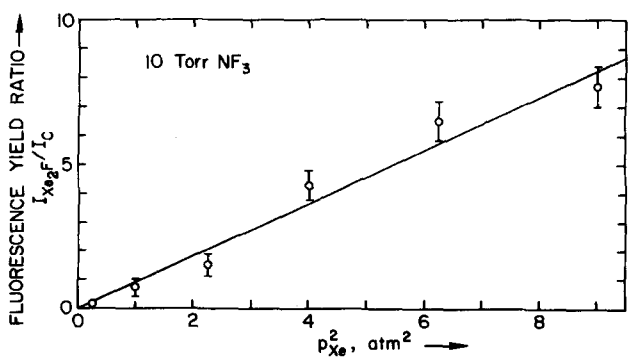

FIG. 15. Fluorescence yield ratio I_{Xe_2F}/I_C as a function of the square of the xenon pressure (p_{Xe}) for a Xe–NF_3 mixture.

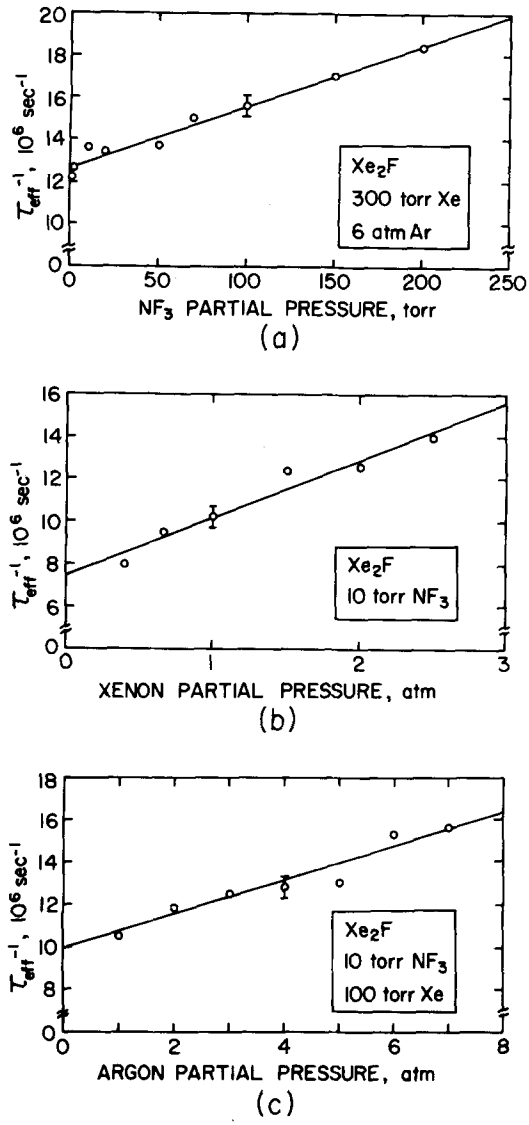

FIG. 16. The decay frequencies of the Xe_2F emission as functions of (a) the NF_3 pressure, (b) the xenon pressure, and (c) the argon pressure.

mined. As in the case of the corresponding quenching constant k_C^{XeXe}, the vibrational distribution is far away from a 300 K Boltzmann distribution and widely unknown. Furthermore, it was assumed that k_{BP}^{XeXe} is negligible as in the case of k_{BP}^{XeAr}. This cannot be shown by fitting solutions of Eq. (3) to a temporal Xe_2F pulse because the collisional coupling in the case of Xe–NF_3 mixtures is so tight that the XeF(B) and the XeF(C) pulse have identical shapes.[30]

Formation rate constants for Xe_2F have been calculated by Shui and Duzy.[43] Due to the lack of reliable potential surfaces for Xe_2F, they did not take into account the possibility of predissociation which might be the reason for the smaller Xe_2F formation rate constants compared to the three-body quenching constants of XeF(C). Therefore, their results should be compared to the three-body quenching constants of XeF(C). In the case of k_C^{XeAr}, good agreement with the present experimental result may be stated (Table I), whereas for k_C^{XeXe} a comparison is not possible because of the high vibrational temperature.

The agreement between the predictions of the kinetic model given in Sec. II and the experimental results is very good. It has, however, been observed by Boewering *et al.*[42] in the case of the ArF–Ar_2F system that for high pumping densities when the exciting current density is above about 1 KA cm^{-2}, deviations from the model underlying Eqs. (1)–(3) may occur. In the case of high excitation densities and high pressures, the buildup of rare gas dimers can compete with ionic reactions forming the rare gas halide dimer molecules. As the rare gas dimers have been shown to be possible precursors of of the rare gas halide trimers[26] in the case of Ar_2F, this might also occur for Xe_2F. In this case, the kinetic equations describing Xe_2F formation have to be extended and can no longer be solved analytically.

In the present experiments, no indications for a possible formation of Xe_2F via Xe_2^* were observed. Such a formation channel should lead to a delayed Xe_2F formation which would create a complicated temporal pulse shape.[42] Instead, pure exponential decays have been always observed for Xe_2F. The decay frequencies have been measured as functions of the partial pressures of the various constituents in the gas mixture. The results are shown in Fig. 16. Straight lines are obtained for every Stern–Volmer plot. The analysis, which is straightforward in this case, leads to the two-body quenching rate constants listed in Table I and a radiative lifetime for Xe_2F of $\tau_X = (152^{+19}_{-10})$ ns.

No indications for a three-body quenching of Xe_2F by NF_3, xenon, or argon, were found (Fig. 16). This justifies neglecting three-body collisions in the definition of τ_{eff}^{-1} in Eq. (3). Furthermore, it indicates that no stable molecules such as Xe_3F or Xe_2ArF are formed by three-body collisions. Since this experimental result was also found for Ar_2F,[40,42] this might be a general feature of all rare gas halide compounds. A possible reason for this behavior is the relative small binding energy of rare gas trimer ions like Ar_3^+ or Xe_3^+ compared to the dimer ions[44] which would lead to unstable Xe_3F molecules and therefore only small three-body quenching constants of Xe_2F would be expected.

V. CONCLUSIONS

When gas mixtures containing high pressure buffer gases are investigated, the analysis of the XeF–Xe_2F kinetic reactions is possible by electron beam excitation or photolysis of Xe_2F. In order to get detailed information about the interaction of vibrational relaxation and collisional mixing and its impact on the XeF_2 formation, a state selective excitation technique similar to those used in Refs. 19 and 21 would be required. However, more theoretical and experimental efforts are necessary in order to understand the magnitude of quenching rates based on the fundamental molecular properties.

Like the other triatomic rare gas halides, Xe_2F is a possible candidate for a tunable excimer laser.[28(b)] Due to its short radiative lifetime and long emission wavelength compared to other trimers, its cross section for

stimulated emission at the emission maximum is relatively high (1.2×10^{-17} cm^2). Also, gain reduction by broadband and narrow band absorbers should be lower in the red part of the visible spectrum than for shorter wavelengths. However, because of the strong xenon quenching of XeF(C), the necessary precursor of Xe_2F, the production efficiency for Xe_2F is considerably lower than for other trimers, which will make it at least very difficult to obtain laser action with Xe_2F.

ACKNOWLEDGMENTS

This work was jointly supported by the Office of Naval Research, the National Science Foundation, and the Robert A. Welch Foundation. The authors wish to thank D. L. Huestis for helpful discussions. R. Sauerbrey would like to acknowledge support by the Deutsche Forschungsgemeinschaft.

[1]C. A. Brau, in *Excimer Lasers*, edited by C. K. Rhodes (Springer, Berlin, 1979).
[2]The notation used in this paper to label the XeF states is the same as that of J. Tellinghuisen, A. K. Hays, J. M. Hoffmann, and G. G. Thisane, J. Chem. Phys. 65, 326 (1976).
[3]E. R. Ault, R. S. Bradford, Jr., and M. L. Bkanimitz, Appl. Phys. Lett. 27, 413 (1975).
[4]C. A. Brau and T. J. Ewing, Appl. Phys. Lett. 27, 435 (1975).
[5]J. C. Hsia, J. A. Mangano, J. H. Jacob, and M. Rokni, Appl. Phys. Lett. 35, 48 (1979).
[6]W. K. Bischel, H. H. Nakano, D. J. Eckstrom, R. M. Hill, D. L. Huestis, and D. C. Lorents, Appl. Phys. Lett. 34, 565 (1979).
[7]N. G. Basov, V. S. Zuev, A. V. Kanaev, L. D. Mikhur, and D. B. Stavroskii, Sov. J. Quantum Electron. 9, 629 (1979).
[8]C. H. Fisher, R. E. Center, G. J. Mullaney, and J. P. McDaniel, Appl. Phys. Lett. 35, 26 (1979).
[9]W. E. Ernst and F. K. Tittel, Appl. Phys. Lett. 35, 48 (1979).
[10]R. Burnham, Appl. Phys. Lett. 35, 48 (1979).
[11](a) W. B. Bischel, D. J. Eckstrom, H. C. Walker, and R. A. Tilton, J. Appl. Phys. 52, 4429 (1981); (b) D. C. Eckstrom and H. C. Walker, Jr., IEEE J. Quantum Electron. **QE-18**, 176 (1982).
[12]J. Liegel, F. K. Tittel, W. L. Wilson, Jr., and G. Marowsky, Appl. Phys. Lett. 39, 369 (1981).
[13](a) J. G. Eden and S. K. Searles, Appl. Phys. Lett. 30, 287 (1977); (b) R. W. Wayant and J. G. Eden, IEEE J. Quantum Electron. **QE-15**, 61 (1979).
[14](a) M. Rokni, J. H. Jacob, J. C. Hsia, and D. W. Trainor, Appl. Phys. Lett. 35, 729 (1979); (b) D. W. Trainor, J. H. Jacob, and M. Rokni, J. Chem. Phys. 72, 3646 (1980); (c) M. Rokni, J. H. Jacob, J. A. Mangano, and R. Brochu, Appl. Phys. Lett. 32, 223 (1978); (d) 30, 458 (1977).
[15](a) J. G. Eden and R. W. Wayant, J. Chem. Phys. 68, 2850 (1978); (b) Opt. Lett. 2, 13 (1978).
[16]R. Burnham and N. W. Harris, J. Chem. Phys. 60, 2742 (1977).
[17](a) H. C. Brashears, Jr. and D. W. Setser, Appl. Phys. Lett. 33, 821 (1978); (b) J. Chem. Phys. 76, 4932 (1982).
[18](a) G. Black, R. L. Sharpless, D. C. Lorents, D. L. Huestis, R. A. Gutcheck, T. D. Bonifield, D. A. Helms, and G. K. Walker, J. Chem. Phys. 75, 4840 (1981); (b) D. C. Lorents, Proceedings of the International Conference on Lasers '81, New Orleans, Louisiana, December 1981.
[19]E. D. Poliakoff, S. H. Southworth, M. G. White, G. Thornton, R. A. Rosenberg, and D. A. Shirley, J. Chem. Phys. 72, 1786 (1980).
[20]R. W. Wayant, Appl. Phys. Lett. 36, 493 (1980).
[21]C. H. Fisher and R. E. Center, J. Chem. Phys. 69, 2011 (1978).
[22]T. H. Dunning and P. J. Hay, J. Chem. Phys. 69, 134 (1978).
[23]D. Kilgler, H. H. Nakano, D. L. Huestis, W. K. Bischel, R. M. Hill, and C. K. Rhodes, Appl. Phys. Lett. 33, 39 (1978).
[24]H. C. Brashears, Jr., D. W. Setser, and Y.-C. Yu, J. Chem. Phys. 74, 10 (1981).
[25]D. C. Lorents, D. L. Huestis, M. V. McCusker, H. H. Nakano, and R. M. Hill, J. Chem. Phys. 68, 4657 (1978).
[26]C. H. Chen, M. G. Payne, and J. P. Judish, J. Chem. Phys. 69, 1626 (1978).
[27]J. A. Mangano, J. H. Jacob, J. Rokni, and A. Hawryluk, Appl. Phys. Lett. 31, 26 (1977).
[28](a) F. K. Tittel, W. L. Wilson, R. E. Stickel, G. Marowsky, and W. E. Ernst, Appl. Phys. Lett. 36, 405 (1980); (b) F. K. Tittel, G. Marowsky, W. L. Wilson, and M. C. Smayling, IEEE J. Quantum Electron. **QE-12**, 2268 (1981).
[29](a) D. L. Huestis, Topical Meeting on Excimer Lasers, Charleston, South Carolina, Sept. 11–13, 1979; (b) D. L. Huestis (private communication).
[30](a) W. Walter, R. Sauerbrey, F. K. Tittel, and W. L. Wilson, Appl. Phys. Lett. 41, 387 (1982); (b) R. Sauerbrey, CLEO Conference, Pheonix, Arizona, April 1982; (c) F. K. Tittel, International Conference on Quantum Electronics, Munich, June 1982.
[31]R. Sauerbrey and H. Langhoff, Appl. Phys. 22, 399 (1980).
[32]D. J. Wren, D. W. Setser, and J. K. Ku, J. Phys. Chem. 86, 284 (1982).
[33]A. L. Smith and P. C. Kolninsky, J. Mol. Spectrosc. 69, 1 (1978).
[34]C. Y. Ny, P. W. Tidemann, B. H. Mahan, and Y. T. Lu, J. Chem. Phys. 66, 5737 (1977).
[35]A. R. Striganow and N. S. Sventitskii, *Tables of Spectral Lines of Neutral and Ionized Atoms* (IFI/Plenum, New York, 1968).
[36]W. L. Wilson, R. A. Williams, R. Sauerbrey, F. K. Tittel, and G. Marowsky, J. Chem. Phys. 77, 1830 (1982).
[37]L. G. Christophorou, D. L. McCorkle, and J. G. Carter, J. Chem. Phys. 54, 253 (1971).
[38]J. Le Calve and M. Bourene, J. Chem. Phys. 56, 6068 (1972).
[39]G. Marowsky, G. P. Glass, F. K. Tittel, and W. L. Wilson, Chem. Phys. Lett. 67, 243 (1979).
[40]G. Marowsky, G. P. Glass, F. K. Tittel, K. Hohla, W. L. Wilson, and H. Weber, IEEE J. Quantum Electron. **QE-18**, 898 (1982).
[41]T. G. Finn, L. J. Palumbo, and L. F. Champagne, Appl. Phys. Lett. 34, 52 (1979).
[42]N. Boewering, R. Sauerbrey, and H. Langhoff, J. Chem. Phys. 76, 3524 (1982).
[43]V. H. Shui and C. Duzy, Appl. Phys. Lett. 36, 135 (1980).
[44]D. L. Turner and D. C. Conway, J. Chem. Phys. 71, 1899 (1979).